Factors Influencing Ligand-Binding Properties of Heme Models: A First Principles Study of Picket-Fence and Protoheme Complexes

Carme Rovira and Michele Parrinello*[a]

Abstract: Two prototype heme models, *protoporphyrin*-IX [Fe(PPIX)] and *picket fence* [Fe(T_{piv}PP)(2-meIm)], are analyzed by density functional theory (DFT) combined with molecular dynamics within the Car–Parrinello scheme (CPMD). The fully optimized structures agree with experiments, help to clarify the structure of the Fe–XY bonds (XY = O_2, CO), and reveal new features like the small displacements of the T_{piv}P substituents to accommodate the bent FeO_2 unit ($\sphericalangle$Fe–O–O = 121°). Structural predictions for [FeT_{piv}PP-(2-meIm)CO] and [Fe(PPIX)] complexes are also provided. A *cis* conformation of the vinyl groups of [Fe-(PPIX)] is favored by 3 kcal mol^{-1}. Electronic and structural properties of the central iron porphyrin are not affected either by the presence of the porphyrin substituents or by the vinyl conformation. Also no change is found with respect to O_2, CO, and NO binding. Structure-energy–spin relations associated with Fe-O-O bending in [Fe-(T_{piv}PP)(2-meIm)(O_2)] are analyzed. Different orientations of the Fe–O_2 bond obtained from the X-ray structure are found to have the same energy. In contrast to protoheme, the picket-fence environment stabilizes the binding of O_2 and CO dramatically, due to electrostatic interactions of the ligand with the polar-binding pocket. The likely influence of a solvation shell on the energetic properties is discussed.

Keywords: carbonyl complexes · density functional theory · dioxygen complexes · heme models · molecular dynamics

Introduction

The oxygen-carrying proteins, hemoglobin (hb) and myoglobin (mb), have often been used as examples of protein conformation, dynamics, and function.[1] The biological function of these proteins (i.e., the binding and release of O_2) takes place in the heme active center and is modulated by a large polypeptide framework.[1] The latter is engineered so as to control the binding of O_2 and discriminate against the binding of endogenous ligands like CO. The interest in elucidating the mechanisms of the protein function has led to a large number of investigations, mainly by means of X-ray, kinetic, thermodynamic, and spectroscopic techniques.[2, 3] As a consequence, many properties of the active center have now been clarified. For example, the FeO_2 bond is bent,[2] whereas FeCO is nearly linear.[3b,c, 10d] It is known that O_2 binding to iron induces significant structural changes, which are closely related to crucial electronic rearrangements.[2]

A parallel line of research has developed involving experiments on synthetic analogues of the active center. A number of iron-porphyrin-containing novel compounds have been synthesized and characterized since the first heme model that reversibly binds oxygen (i.e. the *picket-fence* oxygen complex [Fe(T_{piv}PP)(1,2-MeIm)(O_2)]) was obtained in the early 1970's by Collman and co-workers.[5a–c, 6] The picket strategy is one of the most successful approaches to build heme models.[7] In this approach, the porphyrin is functionalized with bulky groups in order to ensure the selective binding of an axial base (usually an alkyl imidazole or pyridine) and a diatomic molecule (O_2, CO) to the iron atom. In so doing these models mimic the stereochemical properties of myoglobin and hemoglobin[8] and have oxygen affinities similar to the values measured for heme proteins.[4, 7, 9]

An important area of research based on synthetic models is devoted to investigating the factors that determine its ligand-binding affinities. Several studies have shown that structural differences among heme models are able to vary the equilibrium constant (K_{eq}) of the O_2- and CO-binding reaction. These changes have been attributed mainly to hydrogen bonding and polar interactions,[10, 11] but steric interactions, porphyrin distortions and the interplay of various factors have also been proposed.[7, 13, 14]

As an aid to understand these variations, it would be useful to know the structure and strength of the iron–ligand bonds, and how they can be affected by different changes in the axial ligand, porphyrin substituents, solvent, or temperature. Our theoretical study is intended to clarify these aspects.

[a] Prof. M. Parrinello, Dr. C. Rovira
Max-Planck Institut für Festkörperforschung, Heisenbergstrasse 1
D-70569 Stuttgart, (Germany)
Fax: (+49) 711-6891702.
E-mail: parrinello@prr.mpi-stuttgart.mpg.de
E-mail: rovira@prr.mpi-stuttgart.mpg.de, rovira@meiga.qf.ub.es

0947-6539/99/0501-0250 $ 17.50+.50/0

Abstract in Catalan: *En aquest treball s'ha analitzat dos sistemes sovint emprats com a models per l'hemo: protoporfirina-IX i picket-fence, mitjançant la Teoria del funcional de la densitat combinada amb dinàmica molecular, segons l'esquema de Car–Parrinello (CPMD). Les estructures totalment optimitzades d'ambdós sistemes es corresponen amb les dades experimentals. A més, ajuden a clarificar l'estructura dels enllaços Fe–XY (XY = O_2, CO) i posen de manifest detalls com ara els petits desplaçaments dels substituents $T_{piv}P$ per tal d'acomodar el fragment FeO_2 (∢Fe-O-O = 121°). També presentem prediccions estructurals per a $FeT_{piv}PP(2\text{-meIm})CO$ i els complexos de [Fe(PPIX)]. D'entre les dues conformacions, cis o trans, dels grups vinil de [Fe(PPIX)], la primera és 3 kcal mol^{-1} més estable. Tanmateix, les propietats estructurals i electròniques de la porfirina de ferro, així com les propietats d'enllaç respecte a O_2, CO i NO, no es veuen afectades per la presència dels substituents de la porfirina. També hem analitzat les relacions estructura/energia/espín respecte al bending del fragment Fe-O-O en $[Fe(T_{piv}PP)(2\text{-meIm})(O_2)]$. Les diferents orientacions de l'enllaç Fe–O_2 provinents de l'estructura de raigs X tenen la mateixa energia. Al contrari que la molècula de protoporfirina, la picket-fence estabilitza dràsticament l'enllaç d'O_2 i CO, a causa d'interaccions electrostàtiques que s'estableixen entre el lligand i una cavitat d'enllaç fortament polar. També es discuteix sobre la possible influència d'una capa de solvatació en les propietats energètiques.*

Abstract in Italian: *Nell'ambito della teoria del funzionale densità combinata col metodo di dinamica molecolare di Car–Parrinello (CPMD) vengono studiati due modelli prototipo per l'eme: la protoporfirina IX ed il cosidetto picket fence. Le strutture vengono completamente ottimizzate e sono in buon accordo con gli esperimenti. I risulati aiutano a chiarire la struttura del legame Fe–XY (XY = O_2, CO) e rivelano nuovi dettagli, come il piccolo spostamento del sostituente $T_{piv}P$ per far posto al gruppo FeO_2 che è piegato (∢Fe-O-O = 121°). Vengo fatte delle predizioni per la struttura dei complessi $[FeT_{piv}PP(2\text{-meIm})CO]$ e [Fe(PPIX)XY] (XY = O_2, CO, NO). La conformazione cis del gruppo vinilico è energeticamente favorita di 3 kcal mol^{-1}. Le proprietà elettroniche della ferro-porfirina centrale non sono influenzate né dai sostituenti della porfirina né dalla conformazione del vinile. Rimangono anche inalterate le energie di legame con O_2, CO e NO. Viene esaminata la relazione struttura-energia-spin in funzione dell'angolo Fe-O-O in $[Fe(T_{piv}PP)(2\text{-meIm})(O_2)]$. Le differenti orientazioni del legame Fe–O_2 rivelate dalla struttura a raggi X hanno la stessa energia. Le interazioni elettrostatiche del legante con la cavità polare di legame aumentano nel picket fence. Il legame di O_2 e CO diventa drammaticamente piú grande che nel protoeme. Viene discussa la possibile influenza della solvatazione sulla energetica di questi sistemi.*

To date, most of the attempts to model heme by theoretical quantum chemistry methods have been limited to semi-empirical studies on small [FeP] complexes, whose structure has been obtained from the experimental one by setting a planar D_{4h} porphyrin and reorienting the axial ligands along symmetry directions.[16] A few first principles studies on CO and CN complexes of [FeP] have been performed with some degree of structural relaxation,[17b–e] although the fixed structure approximation is still commonly used.[18] We recently reported a study of small heme models without symmetry restrictions, in which binding energies of the Fe–ligand bonds could be also obtained.[19] It was shown that the use of the frozen approximation can lead to serious energetic errors (for instance, geometry optimization of the different spin states of an isolated [FeP] decreases the triplet–quintuplet energy splitting by as much as 20 kcal mol^{-1}).

In this article, we present a first principles study, with no symmetry restrictions, of two systems often used as prototypes of heme models in the literature: iron protoporphyrin IX and iron picket-fence porphyrin. The molecular structures are depicted in Figure 1. [Fe(PPIX)], also called protoheme IX or heme *b*, is the prosthetic group of hemoglobin and myoglobin, as well as other heme proteins such as catalase, peroxidase, and cytochromes. On the other hand, iron picket-fence porphyrin is the most studied heme model from an experimental point of view and it is representative of a large number of molecules based on the same synthetic strategy.[4, 5c] Its O_2 complex, $[FeT_{piv}PP(2\text{-meIm})(O_2)]$, is of major interest as a model for oxymyoglobin. Different chemical groups surround the central iron porphyrin of these systems; this allows us, as a first objective, to investigate the influence of these environments on the ligand-binding properties. Our second objective is to provide precise structural information for these complex systems.

Computational Details

The Car–Parrinello method, based on a combination of a molecular dynamics (MD) algorithm with electronic structure calculations from the density functional theory (DFT),[21a] has already been used with success in the study of systems of biological interest.[20] Our computations were made by means of the generalized gradient-corrected approximation of the spin-dependent density functional theory (DFT-LSD), following the prescription of Becke and Perdew.[21b,c] This choice is consistent with our previous

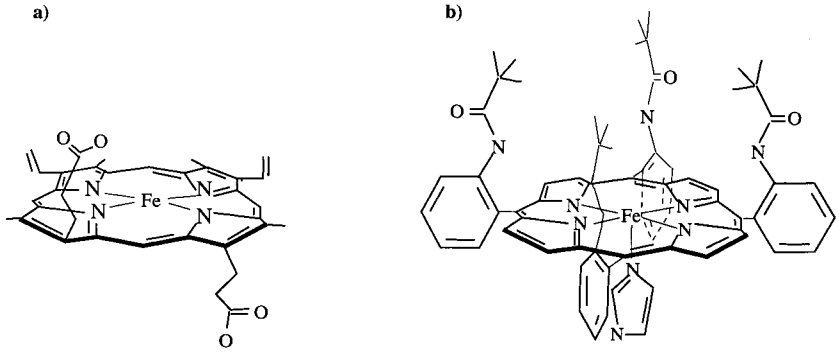

Figure 1. Schematic representation of the two heme models studied. a) Iron-protoporphyrin-IX [Fe(PPIX)]. b) Iron-tetrapivalaminophenyl-2-methyl-imidazole $[Fe(T_{piv}PP)(2\text{-meIm})]$.

work. However, we have verified in selected cases that the use ofthe BLYP functional[21d] leads to very similar results. The relevance of the gradient corrections (GC) for a quantitative understanding of the Fe–ligand-bonding properties (i.e., structure and energy) is given in reference [20f]. Only valence electrons were explicitly included in our computation, and their interaction with the ionic cores was described by norm-conserving, ab initio pseudopotentials generated by means of the scheme developed by Troullier and Martins.[21e] The angular nonlocality was taken into account by the Kleinman–Bylander construction.[21f] The pseudopotential for Fe was supplemented by nonlinear core corrections to enhance the transferability with respect to magnetic excitations.[21g] A previous work on iron porphyrin systems[19] showed that this scheme gives accurate results when compared with all electron DFT calculations. The molecules under study were enclosed in an orthorhombic box periodically repeated in space (box sizes: $a = 14$ Å, $b = 16$ Å, and $c = 12$ Å for the PPIX complexes, $a = c = 19$ Å, $b = 17$ Å for the PF complexes[6]). Single-electron Kohn–Sham (KS) orbitals were expanded in a plane wave basis, with kinetic energy cut-off of 70 Ry (for the computations of PF complexes, this corresponds to 2×10^5 plane waves per KS state, 1.6×10^6 plane waves for the density). Additional computations with larger boxes and cut-off values (80–90 Ry) were performed for selected cases in order to verify the convergence of structures and binding energies.

Results and Discussion

Protoporphhyrin-IX-based systems

1.A. Iron protoporphyrin IX: We performed a complete structural relaxation of the [Fe(PPIX)] molecule in three different spin states: singlet, triplet, and quintuplet ([^{x}Fe(PPIX)], $x = 1$, 3, 5). The initial [Fe(PPIX)] structure (see Figure 2) was taken from our previous [FeP] optimized

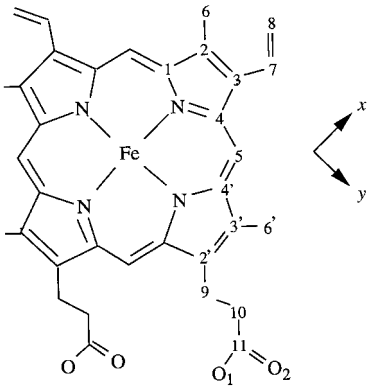

Figure 2. Atom-numbering convention used to define the [Fe(PPIX)] structure.

structure, with the substituent PPIX groups attached in the same orientation as found in the crystal structure of myoglobin.[26] In this structure, the vinyl C=C atoms a *cis* conformation with respect to the C_2–C_3 porphyrin bond, pointing towards the nearest CH_3 substituent.[24] However, the results of resonance Raman measurements for a complex of [Fe(PPIX)] and other vinylhemins have suggested that two torsional isomeric forms of each vinyl are in thermal equilibrium at room temperature.[25] DFT-LDA calculations in small vinyl-substituted molecules and in a Zn^{II} complex of 1,5-dimethyl-2,6-divinylporphyrin support this conclusion, and they give an estimated energy difference between the two isomers of less than 1.28 kcal mol^{-1}.[25]

In order to explore conformational flexibility of the vinyl substituents, additional optimization was performed with one vinyl group with the C_7=C_8 double bond rotated 180° with respect to the C_3–C_7 bond (*trans* conformation, as depicted in Scheme 1). The triplet state [^{3}Fe(PPIX)] turns out to have the

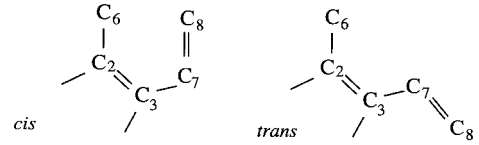

Scheme 1. Vinyl isomerism in [Fe(PPIX)].

lowest energy, as was found for [FeP],[19] and this result is independent of the orientation of the vinyl substituents. Both initial structures converged to a minimum, with the *cis* conformation being more stable by 2.9 kcal mol^{-1}. This energy difference is similar to that found by Kalsbeck et al.[25] in related vinyl-substituted molecules, indicating that this conformational flexibility of the vinyl substituents is a characteristic property of a pyrrolic system.

Table 1 lists the main structural parameters of the optimized [^{3}Fe(PPIX)] structure. For the sake of comparison, the structure of [FeP], computed with the same method,[19] and the structure of the myoglobin heme group[26] are also listed. To the best of our knowledge, no X-ray structure has been reported for a synthetic model based on [Fe^{II}(PPIX)]. Thus, the data in Table 1 is useful as a good approximation for the structure of these synthetic models for which structural information is not yet available.[9, 27] On the other hand, our optimized structure is in good agreement with the structure of the myoglobin prosthetic group. The symmetric pattern of porphyrin C–C bond lengths reflects the aromaticity of the ring (e.g., C_2–$C_3 = C_{2'}$–$C_{3'} = 1.38$ Å). The C–C and C=C bond lengths of the vinyl substituents are 1.45 Å and 1.35 Å, respectively. The nearly D_{4h} iron-porphyrin core of [Fe(PPIX)] has a very similar structure to that when substituent groups are not present. There is a slight out-of-planarity of the porphyrin atoms (the maximum–minimum displacement is 0.1 Å in the outer pyrrolic carbon atoms).

Concerning the electronic structure, there is no direct experimental information available on the ground state of a [Fe(PPIX)] molecule. Nevertheless, related four-coordinate Fe^{II} complexes like Fe^{II}-tetraphenyl-porphyrin ([FeTPP]) are known to have a triplet ground state.[4, 28] The gas-phase [FeP], for which first principles calculations are available, is also in a triplet ground state.[20e, 29] We found that the change in spin state affects only the Fe–N distances, with values of 1.98 Å (triplet and singlet states) and 2.04 Å (quintuplet state). These values are the same as those found for [FeP].[19] The d-orbital occupation of the triplet ground state is $(d_{xy})^2(d_{z^2})^2(d_{xz})^1(d_{yz})^1$ (independently of the vinyl conformation), which was also found for [^{3}FeP]. The computed Mulliken charges of [Fe(PPIX)] and [FeP] are also very similar ($q_{Fe} = 1.0$, $q_N = -0.4$, $q_{C1} = 0.2$, $q_{C5} = -0.2$, $q_H = 0.3$) except for the outer pyrrolic carbon atoms ($q_{C2} = -0.2$ in [FeP] and 0.0 in [Fe(PPIX)], due to a change in one of the covalently attached atoms). Overall, our analysis of the [Fe(PPIX)] molecule reveals that vinyl,

0947-6539/99/0501-0252 $ 17.50+.50/0 *Chem. Eur. J.* **1999**, *5*, No. 1

Table 1. Calculated minimum structure (LSD+GC) of the ground state iron-protoporphyrin ([FePPIX]). The iron porphyrin ([FeP]) and the myoglobin (X-ray) structures are also included. Values in parenthesis refer to the *trans* vinyl group. Distances are in Å and angles in degrees.

	[FePPIX]	[FeP][19]	Myoglobin[26]
iron porphyrin structure[a]			
Fe–N	1.99	1.98	1.90–1.97[b]
N–C_1	1.39	1.39	1.33–1.40
C_1–C_2	1.44	1.44	1.37–1.50
C_2–C_3	1.38	1.36	1.32–1.39
C_4–C_5	1.38	1.38	1.36–1.42
C_5–H	1.09	1.09	–
∢ $FeNC_1$	127.1–128.4	127.6	125.4–130.9
∢ NC_4C_5	124.1–125.3	125.3	123.4–126.1
∢ NC_1C_2	111.1–111.5	110.7	111.4–112.8
∢ $C_1C_2C_3$	105.9–106.3	106.9	102.1–110.6
∢ $C_4C_5C_{4'}$	125.0–125.3	123.8	119.9–126.2
∢ C_4C_5H	116.8–117.9	117.8	–
methyl structure			
C_2–C_6	1.50		1.52–1.55
C_6–H	1.10		–
∢ $C_3C_2C_6$	128.5 (127.5)		127.3–130.4
∢ $C_{2'}C_3C_{6'}$	128.5		128.1–129.7
∢ C_2C_6H	111.2–111.9		–
vinyl structure			
C_3–C_7	1.45		1.41
C_7=C_8	1.35		1.36–1.39
C_7–H	1.10		–
C_8–H	1.09		–
∢ $C_4C_3C_7$	123.1 (129.7)		120.1–121.5
∢ $C_3C_7C_8$	129.0 (130.4)		129.7–130.0
∢ C_3C_7H	115.0 (113.5)		–
∢ C_7C_8H	123.4 (123.4)		–
	119.9 (120.1)		–
τ $C_5C_4C_3C_7$	4.4 (1.4)		4.6–8.2
τ $C_4C_3C_7C_8$	170.6 (–27.4)		149.2–178.8
propionate structure			
C_2–C_9	1.51		1.53
C_9–C_{10}	1.56		1.53
C_{10}–C_{11}	1.51		1.52
C_{11}–O_1	1.22		1.25
C_{11}–O_2	1.37		–
O_1–H	0.99		–
$C_{9,10}$–H	1.10		–

[a] Note that because of the "nearly" D_{4h} symmetry of the iron porphyrin, atoms with the same number are equivalent with respect to the internal [FeP] geometry (e.g., C_2–C_3 = $C_{2'}$–$C_{3'}$). [b] Lowest-highest value found among all distances of this type.

propionate, and methyl substituents do not cause any significant structural distortion and do not affect the electronic structure of its central iron-porphyrin ring.

1.B. Complexes with O_2, CO, and NO: Table 2 lists the main structural parameters of the [Fe(PPIX)] complexes we have studied, in comparison with the nonporphyrin-substituted complexes computed with the same method. Binding energies of the diatomic molecule are also reported. Table 3 displays the computed charges on the atoms, which will be used later on. According to Table 2, neither structural parameters nor binding energies show any significant change with respect to the nonporphyrin-substituted complexes.

The similarity among both [FeP(AB)] and [Fe(PPIX)-(AB)] systems (AB = O_2, CO, NO) is also apparent in the electronic structure. Figure 3 shows the distribution of the

Table 2. Main structural parameters and binding energies computed for the O_2, CO, and NO complexes of [Fe(PPIX)]. Distances are given in Å, angles in degrees, and energies in kcal mol^{-1}.

	[Fe(PPIX)(AB)]	[FeP(AB)]
AB = O_2		
Fe–N_p	2.01	2.01
Fe–O	1.74	1.74
O–O	1.28	1.28
∢ Fe-O-O	124	123
C_{TN}[a]	0.30	0.30
binding energy	9	9
AB = CO		
Fe–N_p	1.99	1.99
Fe–C	1.69	1.69
C–O	1.17	1.17
∢ Fe-C-O	180	180
C_{TN}	0.25	0.33
binding energy	29	26
AB = NO		
Fe–N_p	2.03	2.03
Fe–N	1.69	1.69
N–O	1.19	1.19
∢ Fe-N-O	155	150
C_{TN}	0.38	0.36
binding energy	34	35

[a] Displacement of the Fe atom (towards the diatomic molecule) with respect to the mean plane defined by the porphyrin nitrogens.

Table 3. Calculated atomic charges of the [Fe(PPIX)(AB)] complexes (AB = O_2, CO).[a]

atom	Mulliken	ESP	atom	Mulliken	ESP
PPIX[b]					
N	–0.40	–0.12	C_8	–0.48	–0.50
C_1	0.18	0.05	C_9	–0.45	–0.05
C_2	0.04	0.14	C_{10}	–0.47	–0.25
$C_{2'}$	0.01	–0.06	C_{11}	0.74	0.67
C_3	0.01	–0.10	O_1	–0.63	–0.56
$C_{3'}$	0.03	0.16	O_2	–0.49	–0.56
C_4	0.18	0.08	H_p	0.27	0.17
$C_{4'}$	0.18	0.02	H_m	0.27	0.14
C_5	–0.21	–0.20	H_v	0.28	0.15
C_6	–0.70	–0.51	H_{pr}	0.30	0.10
C_7	–0.22	–0.01	$H(O_1)$	0.54	0.38
CO complex			O_2 complex		
Fe	1.00	0.10	Fe	1.15	0.13
C	0.34	0.27	O_a	–0.11	–0.23
O	–0.39	–0.30	O_b	–0.15	0.07

[a] Because of the similarity among all complexes, only the list of charges on the PPIX atoms is reported. [b] Notation: H_p = porphyrin hydrogen; H_m = methyl hydrogen; H_{pr} = hydrogen attached to propionate carbons (C_9 or C_{10}).

Kohn–Sham orbitals of both [FeP(CO)] and [Fe(PPIX)-(CO)] systems. The two orbital-level distributions share similar features. The molecular levels associated with covalent bonds (σ_{XY}; X, Y = C, O, H, N) appear in the low-energy region. Those corresponding to lone pairs of the oxygen atoms (n_O orbitals) and C=O double bonds (π_{CO}) appear in an intermediate energetic region between the first and d-Fe orbitals, which are mixed with π^* orbitals of CO (Fe → CO π back-bonding). However, the π levels of the vinyl substituents ($\pi_{C=C}$) appear close to the HOMO region, but only weakly mixed with the d-Fe levels.

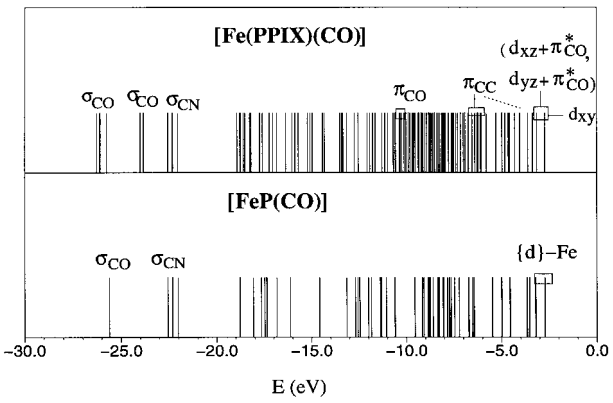

Figure 3. Orbital distribution in [Fe(PPIX)(CO)] (upper pannel) and [FeP(CO)] (lower pannel).

Therefore, we observe that protoheme type of substitution does not change either the properties of an isolated [FeP], nor the main properties of its O_2, CO, and NO complexes. In view of the insensitivity of the coordinated ligand to this type of environment, we have not extended our study to the complexes with an imidazole (Im) ligand. The properties of [Fe(PPIX)(Im)(AB)] are expected to be invariant with respect to the already studied [FeP(Im)(AB)] complexes.[19] On the other hand, the structure of the porphyrin substituents is likely to be very similar to the one reported in Table 1.

2. Picket-fence based systems

2.A. The unligated species: Five-coordinate [FeT_{piv}PP-(*n*-meIm)] complexes ($n=1$, 2) are of interest as synthetic models for deoxymyoglobin. The 2-meIm complex, in particular, is used as a model for the T-form of hemoglobin,[34] since it lowers the O_2- and CO-binding affinities by a power of 10 with respect to the 1-meIm analogue.[7] Our theoretical analysis is based on the former complex, for which a more recent X-ray structure is available.[5d] The molecular structure of [FeT_{piv}PP(2-meIm)] (see Figure 1b) is characterized by the Fe atom being out-of-plane by 0.4 Å with respect to the the mean-plane defined by the four porphyrin nitrogens (hereafter referred as the N_p plane), resulting in large $Fe-N_p$ distances (2.07 Å). The 2-meIm ligand is disordered between two equivalent positions. Concerning the electronic properties, there is general agreement that the iron atom of five-coordinate Fe^{II} models is in a high-spin state ($S=2$), as Mössbauer,[30] NMR,[10f, 31] and magnetic susceptibility measurements have demonstrated.[5d, 32, 33c]

We started our study by performing a single-point calculation with the experimental X-ray structure of the [FeT_{piv}-PP(2-meIm)] molecule considering different spin states. The most stable spin state was found to be a quintet ($S=2$), which is in agreement with experiments. Its corresponding spin density is practically localized on the iron atom, with only a slight amount of σ-spin transfer with the porphyrin ring. Complete relaxation of the molecular structure from CPMD orients the 2-meIm ligand in such a way that its projection on the N_p plane forms an angle of 22.5° with one of the $Fe-N_p$ bonds, which agrees with the experimental value of 22.9°. However, structural relaxation also decreases the iron out-of-planarity (0.1 Å from the experimental value) and, as a consequence, brings the energy of a triplet state below (6 kcal mol^{-1}) that of the quintet. This triplet state exhibits a significant σ-spin transfer between the Fe atom and the porphyrin ring (the spin distribution is $Fe^{2.6\uparrow}-P^{0.6\downarrow}$).

The CPMD electronic structure thus differs from from the well-established $S=2$ state of several five-coordinate ferrous heme models. This surprising discrepancy may arise from several factors. First there is the possibility that the level of theory is not accurate enough. Usually DFT performs well on iron complexes,[17a,d, 18a, 35a] although no calculations on similar five-coordinate Fe^{II} systems have been reported. More intriguing, and of course at this stage more speculative, is the possibility that the structural and electronic properties of the molecules vary when going from the gas to the condensed phase. This effect might arise from the fact that the splitting between the two spin states in the 0 K calculation is rather small. The sensitivity of the spin state to small changes in the Fe out-of-planarity (Δ) was already noted in our previous work, in which slight variations of Δ were found to significantly affect the triplet–quintet energy splitting.[19] Similar spin-structure relations have been discussed for myoglobin, whose Mössbauer spectrum has been interpreted as the mixing of two spin states when the Fe atom undergoes an anharmonic out-of-plane motion of large mean amplitude.[37]

2.B. The complex with oxygen

2.B.1. Electronic and structural properties; dependence on the Fe-O-O angle: We started the structural optimization of the PFO_2 molecule by taking its X-ray structure as a reference.[5d] In order to investigate the orientational preferences of the O_2 ligand, we initially set a linear Fe-O-O angle. The computation was performed on an $S=0$ state within the LSD+GC approximation, which allows either $Fe^{III}-O_2^-$ or $Fe^{II}-O_2$ bonding to occur. After optimizing the structure for a linear Fe-O-O angle (**a**), we relaxed the axial ligands, keeping the rest of the molecule fixed (**b**). In a third step, we optimized the structure with respect to all degrees of freedom (**c**). Scheme 2 illustrates the main structural changes that occur during this process. A quick Fe-O-O bending takes place during step

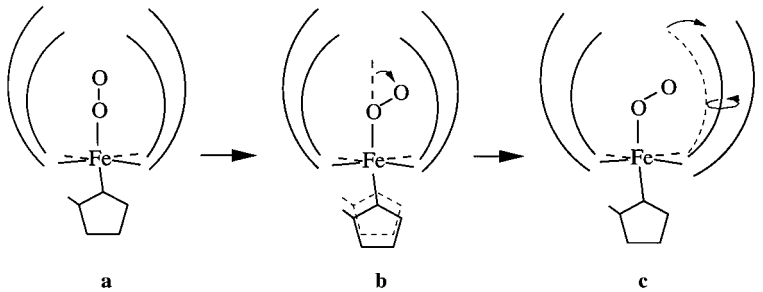

Scheme 2. Main structural changes taking place with O_2 bending in PFO_2.

0947-6539/99/0501-0254 $ 17.50+.50/0 *Chem. Eur. J.* **1999**, *5*, No. 1

a→**b**; the structure evolves rapidly towards a bent Fe-O-O (121°) with the O_2 axis projection in the same porphyrin quadrant as the imidazole. This orientation, defined in more detail in Figure 4, corresponds to one of the four positions

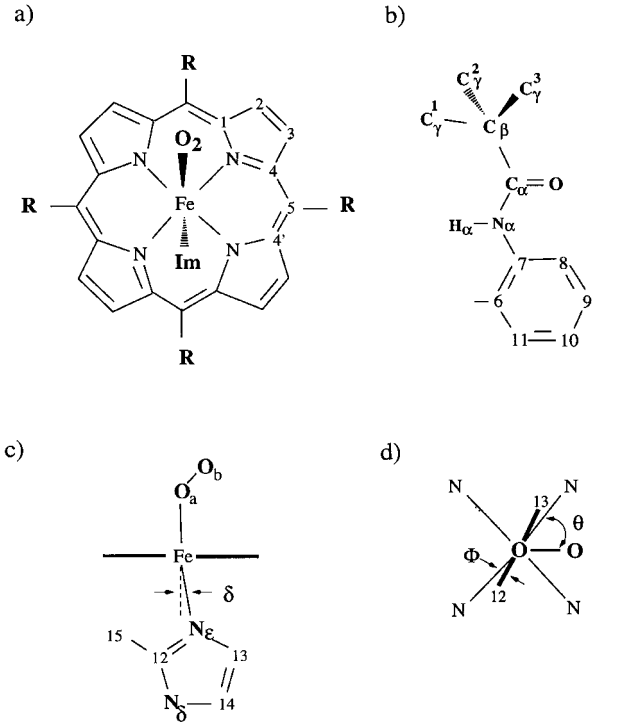

Figure 4. Atom-numbering convention and parameters used to define the [FeT_{piv}PP(2-meIm)(O_2)] structure. a) Iron-porphyrin structure (top view). b) T_{piv}P substituent. c) Orientation of the axial O_2 and imidazole ligands (side view). d) Same as c), view from top.

found experimentally (see Scheme 3) and suggests that orientation **1** could be the global minimum of the system. The relative stability of other minima will be discussed in section 2.B.2.

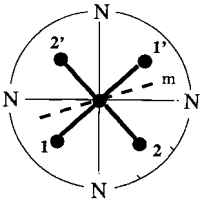

Scheme 3. Different orientations the O_2 and 2-meIm ligands obtained from the X-ray structure.

A small displacement of the porphyrin substituents away from the O_2 molecule occurs during the full relaxation of the molecular structure (step **b**→**c**). This opening of the picket cage, is not equivalent for the four T_{piv}P substituents, but is more pronounced for the one closer to the terminal oxygen, as depicted in Scheme 3. The energetic cost of bending the Fe-O-O angle is very large (26 kcal mol^{-1} in the **a**→**b** step), which indicates that a significant change in Fe–O_2 bonding is involved. In contrast, the energetic cost for the cage opening (**b**→**c**) is very small (6 kcal mol^{-1}). Other changes that occur upon bending are an increase in the O–O bond length (from 1.28 Å in **a** to 1.30 Å in **b**, **c**) and in the Fe–N_ε bond length (from 2.03 Å in **a** to 2.11 Å in **b**, **c**). As a consequence of a longer Fe–N_ε bond, the steric interaction between the imidazole methyl and the porphyrin ring is partially relieved, which decreases the tilting of the imidazole (δ) and the Φ angle by 3° (see the definition of these parameters in Figure 4).[41] Our calculations indicate that changes in the Fe–N_ε bond length are closely related to changes in the Fe-O-O angle and, in turn, to the energy of the Fe–O bond. Before discussing this aspect in detail, it is useful to analyze the changes in the electronic structure of the system.

The origin of the small structural differences we observe when changing the Fe-O-O angle are related to changes in the electronic structure. The d-orbital configuration of Fe in the bent structure (**b** or **c**) is the same as found for a small [FeP(Im)(O_2)] system:[19] an open-shell singlet whose filling of the higher occupied orbitals can be written schematically as $(d_{xy})^{\uparrow\downarrow}(d\pi_1)^{\uparrow\downarrow}(\pi^*_{g,s})^{\uparrow\downarrow}(d\pi_2)^{\uparrow}(\pi^*_{g,a})^{\downarrow}$ (**A**).

This electron distribution follows the semiempirical model proposed by Hoffman et al. in the late 1970's,[42] with some variation due to the spin polarization.[43] In this case one can clearly differentiate these orbitals as having either iron or oxygen character[44] (although a small d_{z^2} component appears in the third orbital, $\pi^*_{g,s}$, its relative contribution is very small). It follows from the above orbital assignment (**A**) that the Fe–O_2 bond can be formally described as Fe^{III}–O_2^-.

The electron distribution in the Fe-O-O linear conformation instead follows the scheme $(d_{xy})^{\uparrow\downarrow}(d_{xz}+\pi^*_{g,1})^{\uparrow\downarrow}(d_{yz}+\pi^*_{g,2})^{\uparrow\downarrow}(d_{xz}-\pi^*_{g,1})^{\uparrow}(d_{yz}-\pi^*_{g,2})^{\downarrow}$ (**B**).

Because of the strong Fe/O_2 mixing, the classification of these orbitals as Fe or O_2 character is not straightforward. Hence, neither the formal description Fe^{III}–O_2^- nor Fe^{II}–O_2 is applicable here. The change in electronic configuration (**A**→**B**), with the total dissapearance of d_{z^2} contribution in the orbitals of **B**, is the cause of the shorter Fe–N_ε distance in the linear structure. The charge transfer into oxygen also disappears, as evidenced by the shorter O–O distance.

All the structure-energy changes discussed up to this point refer to the S = 0 state. However, additional calculations have been performed for higher spin states. The relative energy of these states with respect to Fe-O-O bending is illustrated in Figure 5. It turns out that triplet (S = 1) is the ground state for a linear Fe-O-O conformation, with the same electronic

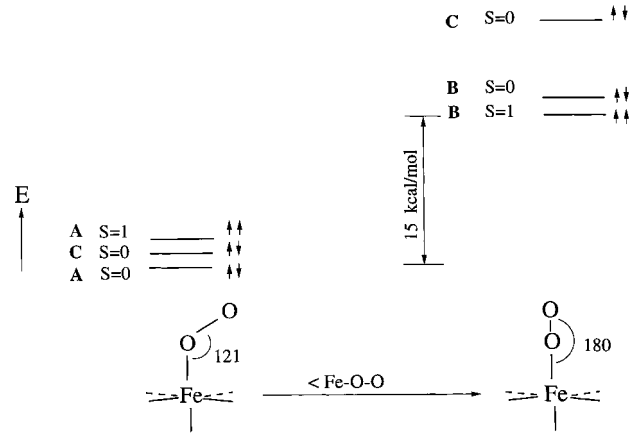

Figure 5. Qualitative picture of the energy among different spin states of [Fe(T_{piv}PP)(2-meIm)(O_2)] as a function of the Fe-O-O angle. Small energy differences are enlarged to improve the visualization (see exact values in the text).

configuration found for the open-shell singlet, $(d_{xy})^{\uparrow\downarrow}(d_{xz}+\pi^*_{g,1})^{\uparrow\downarrow}(d_{yz}+\pi^*_{g,2})^{\uparrow\downarrow}(d_{xz}-\pi^*_{g,1})^{\uparrow}(d_{yz}-\pi^*_{g,2})^{\uparrow}$, thus following Hund's rule.[45] The structural features of this linear Fe-O-O triplet state are the same as those described for the linear Fe-O-O open-shell singlet state (**B**). In the case of the bent ∢Fe-O-O, the lowest triplet state lies only 3 kcal mol^{-1} above the open-shell singlet. Its electronic configuration is very similar to the open-shell singlet state (**A**), with a small mixing of the $d\pi_2$ orbital with d_{xy} as a consequence of the loss of symmetry by bending. The total energetic cost of distorting the FeO_2 moiety from the bent global minimum (S = 0, open-shell) structure to the linear Fe-O-O conformation (S = 1) involves 15 kcal mol^{-1}. Because of this quite high value and the change in spin associated with it, a linear Fe-O-O is unlikely to occur with the room temperature fluctuation of the atomic positions. This excludes it as a transition state for the mechanism of O_2 internal motion among the porphyrin quadrants.

The minimum of the triplet state corresponds to a larger Fe-O-O angle (131°) than that in the singlet state (121°), as we also found in a small [FeP(Im)(O_2)] system.[20f] On the other hand, an S = 0 closed-shell state is well-separated in energy in the linear conformation (22 kcal mol^{-1} with respect to the ground triplet state), but becomes very close to the ground state in the bent conformation (1.4 kcal mol^{-1}). Its electronic configuration can be schematized as $(d_{xy})^{\uparrow\downarrow}\pi^*_{g,s})^{\uparrow\downarrow}(d\pi_1)^{\uparrow\downarrow}(d\pi_2)^{\uparrow\downarrow}$ (**C**) in both conformations. For such a large system, a difference of 1.4 kcal mol^{-1} is at the limit of the accuracy of the method used. Moreover, there is a strong experimental evidence of a diamagnetic state over a wide range of temperatures.[4, 7, 11e,g] Together with the fact that solvation or condensed-matter effects are not not included in our treatment, we cannot differenciate between the two singlet states as being the ground state of the bent FeO_2.

In summary, three spin states (S = 0 open-shell, S = 0 closed shell and S = 1) are in competition as the Fe-O-O angle bends. Although well-separated in energy for a linear Fe-O-O angle, the three spin states become very close (within 3 kcal mol^{-1}), and two of them reverse in energetic order, when the Fe-O-O angle bends. Therefore, there should be a spin crossing region along the Fe-O-O reaction coordinate, in which the three spin states could be mixed by spin–orbit interaction. Since these energy-spin relations are shared with the small [FeP(Im)(O_2)] complex, the existence of these three energetically close spin states seems to be a peculiarity of O_2 binding to a FeP(Im) derivative. On the other hand, our results show that variations in the Fe-O-O angle and Fe–N_ε bond lengths, weakening the Fe–O bond, are closely related to changes in the spin state of the system: a triplet state is favored by a short Fe–N_ε distance and large Fe-O-O angle, while the opposite favors a singlet state. In the context of the protein, this suggests that an appropriate tension through the proximal histidine and/or a steric hindrance opening the Fe-O-O angle could change the spin state of heme.

2.B.2. Minimum-energy structure: The minimum-energy structure parameters of the [FeT_{piv}PP(2-meIm)(O_2)] molecule (i.e., corresponding to a bent Fe-O-O angle) is reported in Tables 4 and 5 (see Figure 4 for the geometry definition). Table 4 lists the most important structural parameters, defin-

Table 4. Main structural parameters computed for the O_2 and CO complexes of [FeP(T_{piv}PP)(2-meIm)]. Distances are given in Å and angles in degrees.

		Calculated	Experimental[5d, 33a]
	PFO_2	[FeP(Im)(O_2)]	
Fe–N_p	2.01	2.01	1.996(4)
Fe–N_ε	2.11	2.08	2.107(4)
Fe–O	1.78	1.77	1.898(7)
O–O	1.30	1.30	> 1.22(2)[a]
∢Fe-O-O	121.0	121.0	< 129(2)
θ	42.6	40	45
δ	4.5	0.0	7.1
C_{TN}[b]	0.04	− 0.07	0.086
N_α–H···O_2	3.09	–	–
	PFCO	[FeP(Im)(CO)]	
Fe–N_p	2.01	2.02	2.02(3)[c]
Fe–N_ε	2.11	2.07	2.10(1)
Fe–C	1.72	1.72	1.77(2)
C–O	1.17	1.17	1.12(2)
∢Fe-C-O	180	180	179(2)
δ	3.8	0.0	–
C_{TN}	0.02	− 0.08	− 0.02

[a] ∢Fe-O-O angle and O–O distance are given as an upper and lower bound respectively. [b] A positive value of C_{tN} indicates a displacement towards the imidazole ligand. [c] Data corresponding to [Fe(TPP)(py)(CO)].[33a]

Table 5. Calculated minimum structure (LSD+GC) of the ground state PFO_2. The isolated [FeP(Im)(O_2)][19] and T_{piv}P structures and the experimental structure of PFO_2 are also included.[5d] Distances are given in Å and angles in degrees.

parameter[a]	PFO_2 calculated	PFO_2 exp[b]	[FeP(Im)(O_2)]
iron porphyrin[c]			
Fe–N	2.01	1.997(4)/1.995(4)	2.01
N–C_1	1.39	1.363(6) – 1.392(6)	1.39
C_1–C_2	1.44	1.424(6) – 1.453(6)	1.44
C_2–C_3	1.36	1.339(7)/1.315(7)	1.36
C_4–C_5	1.40	1.385(6)/1.399(6)	1.38
C_2–H	1.09	–	1.09
∢$FeNC_1$	127.8	127.0(3) – 127.8(3)	127.6
∢NC_4C_5	124.7	125.4(4)/124.9(4)	125.3
∢NC_1C_2	111.3	110.0(4) – 109.8(4)	110.7
∢$C_1C_2C_3$	106.1	106.6(4) – 108.1(4)	106.9
∢$C_4C_5C_{4'}$	125.1	124.5(4)/123.9(4)	123.8
∢$C_4C_5C_6$	117.8	–	117.8
axial imidazole			
N_ε–C_{12}	1.34	1.33	1.39
N_ε–C_{13}	1.39	1.33	1.39
N_δ–C_{12}	1.36	1.32	1.35
N_δ–C_{14}	1.38	1.36	1.38
C_{13}–C_{14}	1.37	1.32	1.37
C_{12}–C_{15}	1.49	1.54	–
C_{13}–H	1.08	–	1.08
C_{14}–H	1.08	–	1.08
C_15–H	1.10		–
N_δ–H	1.02		1.02
φ,δ	20.7,5.2	22.2,7.1	11.5,0.0
∢$FeN_\varepsilon C_{12}$	132.5		127.8
∢$C_{12}N_\varepsilon C_{13}$	106.2	101.6	106.2
∢$C_12N_\delta C_{14}$	109.3	105.4	108.5
∢$C_{13}C_{14}N_\delta$	105.1	105.3	105.6
∢$N_\varepsilon C_{12}C_{15}$	130.3	122.3	–
∢$C_{12}C_{15}$H	110.5	–	–
∢$N_\varepsilon C_{13}$H	121.4	–	121.6
∢$C_{13}C_{14}$H	132.1	–	132.3
∢$C_{12}N_\delta$H	124.4	–	125.8

1999 0947-6539/99/0501-0256 $ 17.50+.50/0 *Chem. Eur. J.* **1999**, *5*, No. 1

Table 5. Continued.

parameter[a]	calculated	PFO_2 exp[b]	[FeP(Im)(O_2)]
porphyrin $T_{piv}P$			
C_α=O	1.23	1.190(7)/1.279(8)	1.23
N_α–C_α	1.38	1.314(7)/1.254(8)	1.38
C_α–C_β	1.55	1.505(9)/1.479(9)	1.55
N_α–H	1.02	–	1.02
C_β–C_γ	1.55	1.42(5)/1.66(5)[d]	1.54
C_γ–H	1.10	–	1.10
N_α–C_7	1.41		1.42
C_6–C_7	1.42		1.41
C_7–C_8	1.41		1.40
C_8–C_9	1.39		1.40
C_9–C_{10}	1.40		1.40
C_{10}–C_{11}	1.40		1.40
C_6–C_{11}	1.40		1.40
$\sphericalangle C_5C_6C_7$	122.9	121.2(5)/120.6(5)	119.7
$\sphericalangle C_8C_7N_\alpha$	122.9	121.1(6)/123.0(6)	122.2
$\sphericalangle C_7N_\alpha C_\alpha$	128.6	128.7(5)/134.1(6)	127.5
$\sphericalangle N_\alpha C_\alpha O$	123.2	120.6(7)/120.6(7)	122.8
$\sphericalangle N_\alpha C_\alpha C_\beta$	116.8	118.3(6)/123.5(7)	
$\sphericalangle C_7N_\alpha H$	115.0	–	115.5
$\sphericalangle C_\alpha C_\beta C_\gamma^1$	114.7	118.0(7)/110.3(7)	114.9
$\sphericalangle C_\alpha C_\beta C_\gamma^2$	106.7	110.5(7)/110.7(7)	107.2
$\sphericalangle C_\alpha C_\beta C_\gamma^3$	106.7	108.2(13)/104.1(10)	106.4
$\sphericalangle C_{11}C_6C_7$	118.5	118.1(5)/119.7(5)	120.4
$\sphericalangle C_{11}C_10C_9$	119.0	119.5(7)/120.8(6)	119.2
$\sphericalangle C_9C_8C_7$	120.4	119.0(7)/119.6(6)	119.6
$\sphericalangle C_7C_8H$	118.5	–	119.4
τ $C_\alpha N_\alpha C_7C_8$	4.9* – 15.0	14.8/28.7	24.0
τ $C_\beta C_\alpha ON_\alpha$	179.5	175.4	180.3

[a] Covalent distances and angles do not show significant differences among the four $T_{piv}P$ substituents (the report value corresponds to the average). Values indicated with an asterisk correspond to the $T_{piv}P$ substituent closer to the terminal oxygen atom. [b] Values in parenthesis correspond to the standard deviation. [c] Note that because of the effective D_{4h} symmetry of the iron porphyrin, atoms with the same number are equivalent with respect to the internal [FeP] geometry (e.g., C_2–C_3 = $C_{2'}$–$C_{3'}$). [d] The large range of values is due to thermal and/or irresolvable disorder.

ing the orientation of the O_2 and 2-meIm ligands. Table 5 reports the internal geometry of the fragments that form the PFO_2 molecule (iron porphyrin, 2-meIm ligand and $T_{piv}P$ substituents). The computed values are compared with the experimental X-ray structure and with the structure of [FeP(Im)(O_2)] and $T_{piv}P$ molecules, computed with the same method. Because of the C_2 symmetry of the X-ray structure, two experimental values are reported in Table 5 for each structural parameter. The computed structure is in good agreement with experimental results. Only slight discrepancies arise in some parts of the structure not precisely known like the FeO_2 internal geometry [O–O (exp) $>$ 1.22, Fe-O-O (exp) $<$ 129°] and the $C(CH_3)_3$ groups of the $T_{piv}P$ substituents, which are affected by thermal motion and/or irresolvable disorder.[5d] Our results reflect a substantial expansion of the O–O distance (1.30 Å) from its gas phase value (1.21 Å), as a consequence of the charge transfer associated with the π back bonding d(Fe) $\rightarrow$ π*(O_2). Figure 6 contrasts the experimental structure (all positions of the disordered O_2 are displayed) with the calculated one. The experimental effective C_2 symmetry structure for the Fe(T_{piv}PP) fragment results from an average over the different orientations of the O_2 ligand

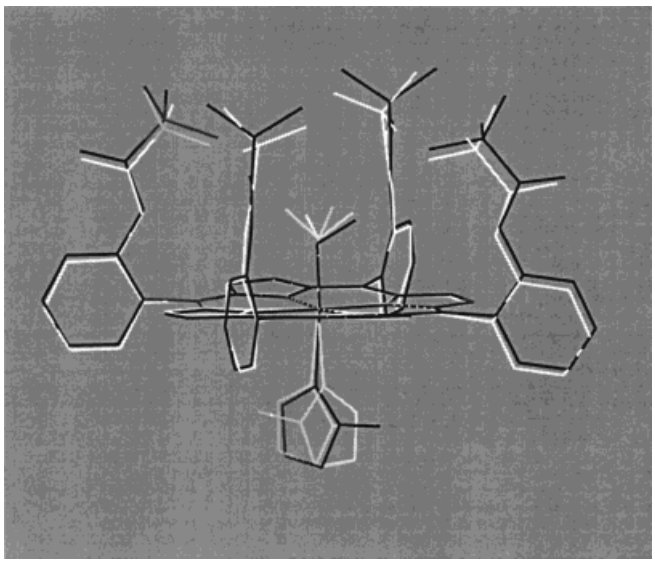

Figure 6. Comparison of the computed [FeT_{piv}PP(2-meIm)(O_2)] structure (black line) with the X-ray structure (white line). The four and two equivalent positions, respectively, for the O_2 and 2-meIm ligands of the crystal structure are shown. Hydrogen atoms of the computed structure have been omitted for clarity.

(see Scheme 3). As a consequence, the displacement of one of the $T_{piv}P$ substituents when the terminal oxygen gets close is not accounted for. This explains why the differences between calculation and experiment are larger for one of the $T_{piv}P$ substituents, as well as for the tilting of the 2-meIm axial ligand. In order to know the relative stability of other minima with respect to O_2 rotation (see Scheme 3), we have performed a structural optimization starting from the PF structure at the first minimum (**1**) and rotating the O_2 molecule according to orientation (**2**).[38] A second local minimum is in fact found at $\theta = 135°$ (see Figure 4). The energy of this minimum lies only 0.2 kcal mol^{-1} higher in energy than the first minimum ($\phi = 45°$). This small energy difference is at the limit of the accuracy of our method, and we conclude that both minima are energetically equivalent. Disregarding the O_2 orientation, the structure of the second minimum (O–O = 1.30 Å, Fe–O = 1.78 Å, $\sphericalangle$Fe-O-O = 120°, Fe–N_p = 2.01 Å, Fe–N_ε = 2.14 Å) is very similar to the first (**1** in Scheme 3). We have performed additional calculations considering an orientation of the oxygen molecule in such a way that its O–O axis projection onto the N_p plane overlaps one of the Fe–N_p bonds. This computation was done by fixing the N_p-Fe-O_1-O_2 dihedral angle and optimizing the structure with respect to all other degrees of freedom. The corresponding optimized structure was found to be only 1.8 kcal mol^{-1} higher in energy than the first minimum (**1** in Scheme 3). Given this small energy difference, rotation of the O_2 ligand around the Fe–O bond (see Scheme 4) at room temperature probably takes place on a short time scale. Temperature effects on the dynamics of O_2 motion will be addressed in a separate publication.[46]

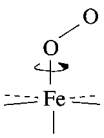

Scheme 4. Most likely mechanism of O_2 motion in PFO_2.

The possibility of the O_2 being hydrogen bonded to the amino group of $T_{piv}P$ is supported by several experimental studies. In particular the NMR chemical shift of the amide hydrogen has been taken as an indication of a hydrogen bond.[11e] The computed H···O distance (3.09 Å and 2.93 Å for the first and second minimum, respectively) is too large to be classified as a hydrogen bond. However, as will be discussed in section 2.D, a significant electrostatic stabilization of the ligand occurs.

In summary, the computed PFO_2 structure is in good agreement with the X-ray structure, and complements it in the determination of several details, like the subtle structural deformations induced by O_2 motion, the structure of the Fe–O_2 and Fe–Im bonding, and the position of hydrogen atoms.

2.C. The complex with carbon monoxide: The picket-fence complex with carbon monoxide, [FeT_{piv}P(2-meIm)(CO)] (hereafter abbreviated as PFCO), is of interest as a synthetic model for the CO complex of myoglobin (mbCO). In this respect, several experimental data for the CO-binding reaction with this picket-fence complex are available.[4] However, unlike its O_2 analogue, the X-ray structure of the PFCO complex has not yet been obtained. The most closely related CO complex for which an X-ray structure has been reported is [FeTPP(py)(CO)], which contains a pyridine molecule instead of imidazole as the axial ligand and lacks the pivalamino substituents.[33a]

The initial structure of the PFCO complex in our study is taken from the minimum-PFO_2 structure, substituting the axial ligand by CO. The calculation is performed with the LDA+GC approximation, since CO heme models are typical examples of low-spin ferrous complexes.[33c] Table 4 reports the main structural parameters defining the equilibrium PFCO structure, in comparison with its O_2 analogue and with the nonsubstituted complex [FeP(Im)(CO)]. The computed data are also compared with the experimental X-ray structure of [FeTPP(py)(CO)]. Despite the structural differences between both molecules, there is a good agreement between the computed structure of PFCO and the experimental structure of [FeTPP(py)(CO)]. The agreement in the Fe–N_ε bond length, however, is likely to be fortuitous. Since pyridine is less basic than imidazole,[11c] the bond should be shorter for imidazole. However the steric hindrance of the 2-me substituent makes it similar to that of pyridine. As in the case of the PFO_2 system, the main [FeP(Im)(CO)] structure is found to be insensitive with respect to the addition of the $T_{piv}P$ substituents (again the only difference is in the Fe–N_ε bond length, which is a consequence of the 2-me group). The main discrepancy between our computed PFCO structure and the experimental [FeTPP(py)(CO)] structure concerns the Fe–C and C–O bond lengths, which are 3 % larger and 4 % shorter, respectively, in the experimental structure (the experimental C–O bond length, 1.12 Å, is, surprisingly, shorter than the value for an isolated CO molecule, 1.13 Å). However, room temperature CPMD simulations showed oscillations of 18° and 12° in the Fe–CO bend and tilting angles, respectively, for a [FeP(Im)(CO)] model.[46] This large librational motion could complicate the structural analysis and lead to an apparently shorter CO bond, reflecting the projection of the CO bond on the librational axis and not its true bond length. A linear Fe-C-O bond is found in the experimental [FeTPP(py)(CO)] structure and in the three CO complexes of [FeP] that we have studied to date (PFCO, [FeP(Im)(CO)], and [FeP(CO)]). Related heme – CO synthetic models also show a linear CO.[33b] The detailed structure of the PFCO complex is reported in Table 6. Although the data show little change with respect to the PFO_2 system, it can be useful as an approximation to the unknown structure of this CO complex.

2.D. Strength of Fe diatomic bonds: The computed binding energy of the picket-fence complexes with CO and O_2 is reported in Table 7. We also include the results obtained, with the same method, for the nonsubstituted systems ([FeP(Im)(AB)] and [FeP(AB)], AB = O_2, CO). The values of Table 7 show that the strength of ligand binding is significantly enhanced by the $T_{piv}P$ substituents. The energy increase (32 kcal mol^{-1} for O_2 and 28 kcal mol^{-1} for CO) is larger that observed with the addition of an imidazole axial ligand (6 kcal mol^{-1} and 9 kcal mol^{-1}, respectively) and contrasts with the results obtained for protoheme complexes (Table 2), in which the binding energy is not affected by this particular porphyrin substitution.

The origin of the different behavior between the picket fence and protoheme is probably related to the polarity of the porphyrin substituents. In the case of the picket fence, the dipole moment of the amide groups of each $T_{piv}P$ is oriented towards the diatomic ligand, which results in a stabilizing interaction with the dipole of the FeO_2 or FeCO fragments. In the case of [Fe(PPIX)], the polar acidic groups (see Figure 1a) are far from the ligand position (5 – 7 Å from the terminal atom of the diatomic ligand). Moreover, due to their relative position (on opposite sides of the porphyrin) the total electrostatic interaction with the diatomic would vanish.

An estimation of the electrostatic interaction between the diatomic molecule and the porphyrin substituents can be obtained from the computed charges on the atoms (Table 8). Using a simple formula, $U = \Sigma q_i \cdot q_j / R_{ij}$, we obtained a large stabilizing interaction of the ligand in the picket-fence complexes (21 kcal mol^{-1} for O_2 and 15 kcal mol^{-1} for CO), but almost negligible in the protoheme complexes. Since we did not observe changes in the Fe–O and Fe–C bond orders on attaching the picket substituents, we conclude that electrostatic interactions are the responsible for the large increase in binding energy. That the environment could play a major role in controlling the ligand binding to iron in heme models and, probably, also in myoglobin is in agreement with the conclusions of site-directed mutagenesis experiments[3a] and the recent evidence for the high oxygen affinity of Ascaris hemoglobin.[15] The stabilizing effect of a polar environment is also consistent with measurements of ligand-binding affinities in heme models.[4, 7, 10, 14] Although there is a wide range of measurements in the literature, low affinities are found, in general, for binding pockets of low polarity.[10, 14] An example of the significant influence of the binding-pocket polarity and stereochemistry is provided by the high O_2 affinity recently found in dendrite porphyrins.[10e]

0947-6539/99/0501-0258 $ 17.50+.50/0 *Chem. Eur. J.* **1999**, *5*, No. 1

Table 6. Calculated minimum structure (LSD+GC) of the ground state [FeP(T_{piv}PP)(2-meIm)(CO)] (PFCO). The isolated [FeP(Im)(CO)][19] is also included. Distances are given in Å and angles in degrees.

parameter[a]	[Fe(T_{piv}PP)(2-meIm)(CO)]	[FeP(Im)(CO)]
iron porphyrin[b]		
Fe–N	2.01	2.02
N–C_1	1.38	1.39
C_1–C_2	1.45	1.44
C_2–C_3	1.36	1.36
C_4–C_5	1.40	1.38
C_2–H	1.09	1.09
$\sphericalangle$ FeNC_1	127.0	127.6
$\sphericalangle$ NC_4C_5	126.0	125.3
$\sphericalangle$ NC_1C_2	110.2	110.7
$\sphericalangle$ $C_1C_2C_3$	107.0	106.9
$\sphericalangle$ $C_4C_5C_{4'}$	123.4	123.8
$\sphericalangle$ $C_4C_5C_6$	118.8	117.8
axial imidazole		
N_ε–C_{12}	1.34	1.39
N_ε–C_{13}	1.39	1.39
N_δ–C_{12}	1.37	1.35
N_δ–C_{14}	1.38	1.38
C_{13}–C_{14}	1.38	1.37
C_{12}–C_{15}	1.49	–
C_{13}–H	1.08	1.08
C_{14}–H	1.08	1.08
C_{15}–H	1.10	–
N_δ–H	1.02	1.02
θ, δ	22.8,3.8	11.5,0.0
$\sphericalangle$ FeN$_\varepsilon C_{12}$	133.8	127.8
$\sphericalangle$ $C_{12}N_\varepsilon C_{13}$	106.1	106.2
$\sphericalangle$ $C_{12}N_\delta C_{14}$	109.2	108.5
$\sphericalangle$ $C_{13}C_{14}N_\delta$	105.1	105.6
$\sphericalangle$ N$_\varepsilon C_{12}C_{15}$	130.2	–
$\sphericalangle$ $C_{12}C_{15}$H	110.5	–
$\sphericalangle$ N$_\varepsilon C_{13}$H	121.6	121.6
$\sphericalangle$ $C_{13}C_{14}$H	132.1	132.3
$\sphericalangle$ $C_{12}N_\delta$H	124.4	125.8
T_{piv}P		
C_α=O	1.23	1.23
N_α–C_α	1.38	1.38
C_α–C_β	1.55	1.55
N_α–H	1.02	1.02
C_β–C_γ	1.54	1.54
C_γ–H	1.10	1.10
N_α–C_7	1.41	1.42
C_6–C_7	1.42	1.41
C_7–C_8	1.41	1.40
C_8–C_9	1.39	1.40
C_9–C_{10}	1.40	1.40
C_{10}–C_{11}	1.40	1.40
C_6–C_{11}	1.40	1.40
$\sphericalangle$ $C_5C_6C_7$	122.5	119.7
$\sphericalangle$ $C_8C_7N_\alpha$	121.8	122.2
$\sphericalangle$ $C_7N_\alpha C_\alpha$	128.4	127.5
$\sphericalangle$ $N_\alpha C_\alpha$O	123.2	122.8
$\sphericalangle$ $N_\alpha C_\alpha C_\beta$	116.8	
$\sphericalangle$ C_7N_αH	114.8	115.5
$\sphericalangle$ $C_\alpha C_\beta C^1_\gamma$	114.7	114.9
$\sphericalangle$ $C_\alpha C_\beta C^2_\gamma$	107.1	107.2
$\sphericalangle$ $C_\alpha C_\beta C^3_\gamma$	106.4	106.4
$\sphericalangle$ $C_{11}C_6C_7$	118.6	120.4
$\sphericalangle$ $C_{11}C_{10}C_9$	119.1	119.2
$\sphericalangle$ $C_9C_8C_7$	120.4	119.6
$\sphericalangle$ C_7C_8H	118.7	119.4
τ $C_\alpha N_\alpha C_7C_8$	15.4	24.0
τ $C_\beta C_\alpha ON_\alpha$	178.5	180.3

[a,b] See footnotes [a] and [c] of Table 5.

Table 7. Binding energies (kcal mol^{-1}) of the picket-fence complexes investigated and related nonporphyrin-substituted complexes,[21] with respect to O_2 and CO dissociation.

O_2 complex	ΔE	CO complex	ΔE
[Fe(T_{piv}PP)(2-meIm)(O_2)]	47	[Fe(T_{piv}PP)(2-meIm)(CO)]	63
[FeP(Im)(O_2)]	15	[FeP(Im)(CO)]	35
[FeP(O_2)]	9	[FeP(CO)]	26

Table 8. Calculated atomic charges of the [Fe(T_{piv}PP)(2-meIm)(AB)] complexes (AB = O_2, CO).[a]

Atom	Mulliken	ESP	Atom	Mulliken	ESP
porphyrin[b]					
N_p	–0.40	–1.10	C_4	0.17	0.04
C_1	0.17	0.04	C_5	–0.04	–0.25
C_2	–0.22	–0.20	H	0.31	0.13
C_3	–0.22	–0.20			
T_{piv}P[c]					
N_α	–0.55	–0.70	C_7	0.17	0.31
C_α	0.70	0.54	C_8	–0.22	–0.21
O	–0.66	–0.60	C_9	–0.22	–0.24
H_α	0.53	0.28	C_{10}	–0.23	–0.10
C_β	0.00	0.92	C_{11}	–0.21	–0.34
C_γ	–0.72	–0.50	H_v	0.31	0.18
C_6	0.00	0.28	H_m	0.29	0.14
imidazole					
N_ε	–0.37	–0.70	C_{14}	–0.13	–0.16
N_δ	–0.47	–0.18	C_{15}	–0.68	–0.77
C_{12}	0.38	0.49	H	0.35	0.22
C_{13}	–0.08	–0.14	H_m	0.29	0.20
	Fe–CO bond			Fe–O_2 bond	
Fe	1.00	2.80	Fe	1.20	3.04
C	0.45	–0.63	O_a	–0.11	–0.50
O	–0.52	–0.10	O_b	–0.15	0.25

[a] Because of the similarity among both complexes, the charges on the atoms of T_{piv}P, porphyrin, and axial imidazole are reported only once. [b] See atom labeling in Figure 5. [c] Notation: H_m = methyl hydrogen; H_v = methylene hydrogen.

The computed values show the same trend as the experiments, although a quantitative comparison with our gas-phase results is not possible. The large energy increase[47] we observe with the polar picket environment (Table 7) can be regarded as an extreme situation in which electrostatic effects play an exaggerated role in the strength of ligand binding. However, additional factors would contribute to this strength in a protein environment and in solution. Once the molecules are embedded in a solvent, it is likely that the large electrostatic effect of the immediate environment that we find for the gas-phase PF complexes is reduced (the large values of the dipole moment we found for the gas-phase molecules, 10–16 D, gives support to this assumption).[48] Inspection of the computed electrostatic potential of the PFCO molecule (Figure 7) shows that regions of maximum positive potential are localized in the C–C and C–N bonds, whereas a large region of maximum negative potential (red) is located around each amide oxygen atom. This outer negative region would act as a good proton acceptor in the interaction with the solvent molecules (the oxygen atom of the CO ligand, located in a region of weak negative potential, is expected to be a poorer acceptor than the amide oxygens). Specific T_{piv}P–solvent interactions will probably screen the

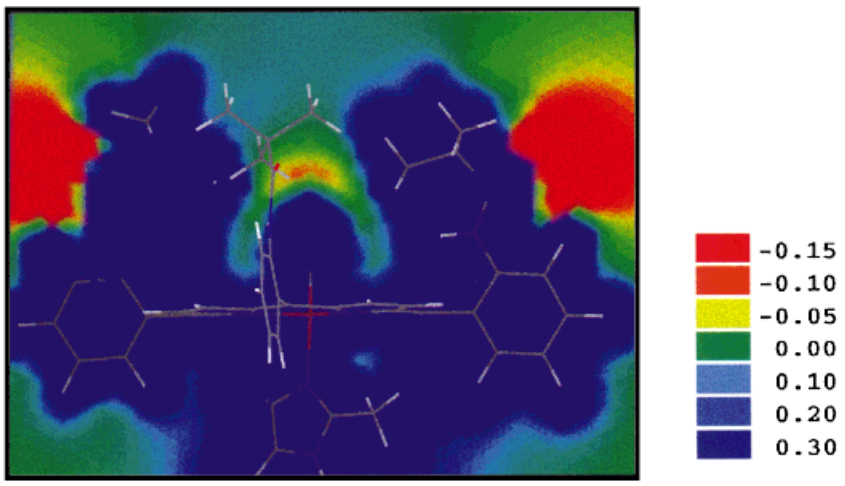

Figure 7. Electrostatic potential map (au) for a [FeT$_{piv}$PP(2-meIm)(CO)] molecule. The plot corresponds to a slice along z which contains, approximately, two of the T$_{piv}$P groups.

charges on the T$_{piv}$P substituents and thus reduce their electrostatic interaction energy with the coordinated O_2 and CO ligands.

In summary, our results show a dramatic stabilization of the diatomic ligand due to the polarity of the binding pocket. However, an important contribution to the binding energy is likely to be due to solvation effects, and including these effects is therefore essential to calculate binding energies comparable with experimental values in solution. This calculation is not yet possible by ab initio methods, but the problem would be well suited for approaches based on mixed ab initio/force-field MD methods, which we are currently starting to apply.

Conclusion

The study reported here constitutes a quantitative analysis of the interplay between energetic, structural, and electronic properties of iron-protoporphyrin IX (protoheme) and [Fe(T$_{piv}$PP)] (picket fence) heme models, and comparison with simpler [FeP(Im)(AB)] and [FeP(AB)] models by means of DFT-based MD within the Car–Parrinello scheme. The analysis of [Fe(PPIX)] (i.e., the myoglobin active center) and its complexes with O_2, CO, and NO reveals that the local environment provided by this particular type of porphyrin substitution does not affect the main chemical properties of ligand binding to the iron porphyrin. The porphyrin ring is practically undistorted, with bond lengths and angles unchanged compared with the calculation of [FeP] alone. Binding energies of the diatomic molecule (Fe–O_2 = 9 kcal mol^{-1}; Fe–CO = 26 kcal mol^{-1}, and Fe–NO = 36 kcal mol^{-1}) do not show variation with respect to the corresponding [FeP(AB)] complexes. The orbitals centered on the porphyrin vinyl substituents are found to be near the HOMO region, but are not strongly mixed with the d-Fe orbitals. Each vinyl substituent prefers a *cis* conformation with respect to its neighboring methyl substituent (with a 3 kcal mol^{-1} difference with respect to its *trans* isomer). Our optimized structures for [Fe(PPIX)] and its complexes can be used as a prediction for the structures of Fe^{II}-protoheme heme models.

Picket-fence complexes have been more thoroughly studied due to the larger amount of experimental information available. The optimized structures of [FeT$_{piv}$P(2-meIm)(AB)] (AB = O_2, CO) are in agreement with the available X-ray structures. In the case of the CO complex, our results can also be used to predict the structure of the [Fe(T$_{piv}$PP)(2-meIm)(CO)] model, whose X-ray structure its not known. In the case of the O_2 complex, our structural results (Fe–O = 1.78 Å, O–O = 1.30 Å, and $\sphericalangle$Fe-O-O = 121°, independently of the presence of the T$_{piv}$P substituents) help to clarify the structure of the FeO_2 fragment (O–O (exp) > 1.22, Fe-O-O (exp) < 129°). The T$_{piv}$P substituents are found to undergo small movements to accommodate the diatomic ligand. Two energetically equivalent local minima are found, with the O–O axis projection either in the same quadrant of the projection of the axial imidazole or in a different quadrant. This explains the statistical equivalence of both orientations in the X-ray crystal structure. Since the orientation in which O–O eclipses one of the Fe–N$_p$ bonds is found to be only 1.8 kcal mol^{-1} higher in energy, easy rotation of the axial ligand at room temperature is predicted. Analysis of the Fe-O-O bending in PFO_2 reveals interesting features linking its structural, energetic, and electronic properties. While a singlet ground state is found for the minimum-bent structure, a triplet state (with a different orbital configuration) is stabilized as the Fe-O-O opens and, simultaneously, the bond length to the axial imidazole (Fe–N$_\varepsilon$) decreases. These properties, which are found to be common in the O_2 binding to a [FeP] derivative, underline the sensitivity of the spin state to subtle structural changes. The strength of O_2 and CO binding to iron in a picket-fence type of environment is enhanced significantly (28–30 kcal mol^{-1}) with respect to the nonsubstituted complexes, in contrast with the situation in the protoheme environment. This is due mainly to electrostatic interactions of the ligand with the polar-binding pocket, as evidenced by the estimation of the electrostatic interaction using the computed atomic charges. Thus, while structures are maintained with respect to environmental changes (even in the presence of the bulky T$_{piv}$P substituents), binding energies are extremely sensitive to the polarity of the binding pocket. The huge electrostatic effect provided by the picket-fence cage is expected to be reduced once solvation effects are taken into account. We are currently completing a study of the O_2 dynamics in the [FeT$_{piv}$P(2-meIm)(O_2)] molecule and planning the modeling of the solvent–picket interaction.

0947-6539/99/0501-0260 $ 17.50+.50/0 *Chem. Eur. J.* **1999**, *5*, No. 1

Acknowledgments

We thank the Garching Computer Center (Garching, Germany) for their support. C. Rovira acknowledges the financial support of the Training and Mobility of Researchers programme of the European Union under contract No. ERBFMBICT96-0951. We acknowledge P. Ballone, J. Hütter, and especially M. Klein for useful discussions. We also thank one of the referees for many interesting suggestions.

[1] L. Stryer, *Biochemistry*, 4th ed., Freeman, New York, **1995**.
[2] a) M. F. Perutz, G. Fermi, B. Luisi, B. Shaanan, R. C. Liddington, *Acc. Chem. Res.* **1987**, *20*, 309; b) B. Shaanan, *J. Mol. Biol*. **1983**, *171*, 31; c) J. S. Olson, G. N. Phillips, *J. Biol. Chem.* **1996**, *271*, 17593.
[3] a) B. A. Springer, S. G. Sligar, J. S. Olson, G. N. Phillips, *Chem. Rev.* **1994**, *94*, 699; b) I. Schlichting, J. Berendzen, G. N. Phillips, R. M. Sweet, *Nature* **1994**, *371*, 808; c) M. Lim, T. A. Jackson, P. A. Anfirud, *Science* **1995**, *269*, 962; d) C. Slebodnick, J. A. Ibers *J. Biol. Inorg. Chem.* **1997**, *2*, 521.
[4] M. Momenteau, C. A. Reed, *Chem. Rev.* **1994**, *94*, 659.
[5] a) J. P. Collman, R. R. Gagne, T. R. Halbert, J. C. Marchon, C. A. Red, *J. Am. Chem. Soc*. **1973**, *95*, 7868; b) J. P. Collman, J. L. Hoard, N. Kim, G. Lang, C. A. Reed, *J. Am. Chem. Soc*. **1975**, *97*, 2676; c) J. P. Collman, R. R. Gagne, C. A. Reed, T. R. Halbert, G. Lang, W. T. Robinson, *J. Am. Chem. Soc*. **1975**, *97*, 1427; d) G. B. Jameson, F. Molinaro, J. A. Ibers, J. P. Collman, J. I. Brauman, E. Rose, K. S. Suslick, *J. Am. Chem. Soc* **1980**, *102*, 3224.
[6] Abbreviations: P = porphyrin; $T_{piv}P$ = tetrapivalaminophenyl; 2-meIm = 2-methylimidazole; (PPIX) = protoporphyrin IX ; PF = [Fe(T_{piv}PP)-(2-meIm)]; PFO_2 = [Fe(T_{piv}PP)(2-meIm)(O_2)]; PFCO = [Fe(T_{piv}PP)-(2-meIm)(CO)].
[7] J. P. Collman, *Inorg. Chem.* **1997**, *36*, 5145.
[8] M. F. Perutz, S. S. Hasnain, P. J. Duke, J. L. Sessler, J. E. Hahn, *Nature* **1982**, *295*, 535.
[9] T. G. Traylor, *Acc. Chem. Res.* **1981**, *102*.
[10] a) K. S. Suslick, M. M. Fox, *J. Am. Chem. Soc*. **1983**, *105*, 3507; b) J. P. Collman, J. I. Brauman, B. L. Iverson, J. L. Sessler, R. M. Morris, Q. H. Gibson, *J. Am. Chem. Soc*. **1983**, *105*, 3052; c) D. Lexa, M. Momenteau, J. M. Saveant, F. Xu, *J. Am. Chem. Soc*. **1986**, *108*, 6937; d) G. B. Ray, X.-Y. Li, J. A. Ibers, J. L. Sessler, T. G. Spiro, *J. Am. Chem. Soc*. **1994**, *116*, 162; e) J. P. Collman, L. Fu, A. Zingg, F. Diederich, *Chem. Commun*. **1997**, 193; f) J. P. Collman, X. Zhang, K. Wong, J. I. Brauman, *J. Am. Chem. Soc*. **1994**, *116*, 6245.
[11] a) J. Mispelter, M. Momenteau, D. Lavalette, J.-M. Lhoste, *J. Am. Chem. Soc*. **1983**, *105*, 5165; b) G. B. Jameson, R. S. Drago, *J. Am. Chem. Soc*. **1985**, *107*, 3017; c) M. Momenteau, B. Loock, D. Lavalette, C. Tetreau, J. Mispelter, *J. Chem. Soc. Chem. Commun.* **1983**, 962; d) G. E. Wuenschell, C. Tetreau, D. Lavalette, C. A. Reed, *J. Am. Chem. Soc*. **1992**, *114*, 3346; e) I. P. Gerothanassis, M. Momenteau, B. Loock, *J. Am. Chem. Soc*. **1989**, *111*, 7006; f) K. Spartalian, G. Lang, J. P. Collman, R. R. Gagne, C. A. Reed, *J. Chem. Phys*. **1975**, *63*, 5375; g) E. Oldfield, H. C. Lee, C. Coretsopoulos, F. Adebodum, K. D. Park, S. Yang, J. Chung, B. Phillips, *J. Am. Chem. Soc*. **1991**, *113*, 8680.
[12] J. P. Collman, J. I. Brauman, T. J. Collins, B. Iverson, J. L. Sessler, *J. Am. Chem. Soc*. **1981**, *103*, 2450.
[13] a) J. P. Collman, P. C. Herrmann, L. Fu, T. A. Eberspacher, M. Eubanks, B. Boitrel, P. Hayoz, X. Zhang, J. I. Brauman, V. W. Day, *J. Am. Chem. Soc*. **1997**, *119*, 3481; b) A. Desbois, M. Momenteau, M. Lutz, *Inorg. Chem*. **1989**, *28*, 825.
[14] J. A. Ibers, *Comments Inorg. Chem*. **1983**, *2*, 97.
[15] S. Huang, J. Huang, A. P. Kloek, D. E. Goldberg, J. M. Friedman, *J. Biol. Chem*. **1996**, *271*, 958.
[16] See, for instance: a) D. A. Case, B. H. Huynh, M. Karplus, *J. Am. Chem. Soc*. **1979**, *101*, 4433; b) R. F. Kirchner, G. H. Loew, *J. Am. Chem. Soc*. **1977**, *99*, 4639; c) J. E. Newton, M. B. Hall, *Inorg. Chem*. **1984**, *23*, 4627; d) G. H. Loew, R. F. Kirchner, *Int. J. Quantum Chem. Quantum Biol. Symp.* **1978**, *5*, 403; e) Z. S. Herman, G. H. Loew, *J. Am. Chem. Soc*. **1980**, *102*, 1815; f) D. C. Doetschman, *Chem. Phys.* **1980**, *48*, 307; g) A. Waleh, H. Nan, L. Chantranupong, G. H. Loew, *J. Am. Chem. Soc*. **1989**, *111*, 2767; h) W. D. Edwards, B. Weiner, M. C. Zerner, *J. Am. Chem. Soc*. **1986**, *108*, 2196.
[17] a) A. Ghosh, J. Almlof, Q. Lawrence, *J. Phys. Chem*. **1994**, *98*, 5576; b) A. Ghosh, D. F. Bocian, *J. Phys. Chem*. **1996**, *100*, 6363; c) P. Jewsbury, S. Yamamoto, T. Minato, M. Saito, T. Kitagawa, *J. Phys. Chem*. **1995**, *99*, 12677; d) R. H. Havlin, N. Godbout, R. Salzmann, M. Wojdelski, W. Arnold, C. E. Schulz, E. Oldfield, *J. Am. Chem. Soc*. **1998**, *120*, 3144; e) T. Vangberg, D. Bocian, A. Ghosh, *J. Biol. Inorg. Chem*. **1997**, *2*, 521.
[18] a) H. Kuramochi, L. Noodleman, D. A. Case, *J. Am. Chem. Soc*. **1997**, *119*, 11442; b) Y. Tokita, H. Nakatsuji, *J. Phys. Chem. B* **1997**, *101*, 3281; c) J. Antony, M. Grodzicki, A. X. Trautwein, *J. Phys. Chem. A* **1997**, *101*, 2692.
[19] C. Rovira, K. Kunc, J. Hutter, P. Ballone, M. Parrinello, *J. Phys. Chem. A* **1997**, *101*, 8914.
[20] a) P. Carloni, W. Andreoni, *J. Phys. Chem*. **1996**, *100*, 17797; b) M. Marchi, J. Hutter, M. Parrinello, *J. Am. Chem. Soc*. **1996**, *118*, 7847; c) J. Hutter, P. Carloni, M. Parrinello, *J. Am. Chem. Soc*. **1996**, *118*, 8710; d) D. E. Sagnella, K. Laasonen, M. L. Klein, *Biophys J*. **1996**, *71*, 1172; e) C. Rovira, P. Ballone, M. Parrinello, *Chem. Phys. Lett*. **1997**, *271*, 247; f) C. Rovira, M. Parrinello, *Int. J. Quant. Chem*. **1998**, *70*, 387.
[21] a) See for instance: G. Galli, M. Parrinello, *Computer Simulation in Materials Science*, (Ed.: V. Pontikis, M. Meyer) Kluwer, Dordrecht, **1991**, and references therein; b) A. D. Becke, *J. Chem. Phys*. **1986**, *84*, 4524; c) J. P. Perdew, *Phys. Rev. B* **1986**, *33*, 8822; d) C. Lee, W. Yang, R. G. Parr, *Phys. Rev. B*. **1988**, *37*, 785; e) N. Troullier, J. L. Martins, *Phys. Rev. B* **1991**, *43*, 1993; f) L. Kleinman, D. M. Bylander, *Phys. Rev. Lett*. **1982**, *48*, 1425; g) S. G. Louie, S. Froyen, M. L. Cohen, *Phys. Rev. B* **1982**, *26*, 1738; h) I. Stich, R. Car, M. Parrinello, S. Baroni, *Phys. Rev. B* **1989**, *39*, 4997; i) J. Hutter, H. P. Lüthi, M. Parrinello, *Comput. Mat. Sci*. **1994**, *2*, 244.
[22] a) The list of atomic coordinates for all the computed structures are available by anonymous ftp (address: parrix1.mpi-stuttgart.mpg.de, directories: pub/outgoing/Fe(PPIX) and /pub/outgoing/FePF); b) Computations have been performed by the CPMD program version 3.0, written by J. Hutter, Max-Planck-Institut für Festkörperforschung, Stuttgart, **1996**.
[23] a) L. E. Chirlian, M. M. Francl, *J. Comp. Chem*. **1987**, *8*, 894. b) ESP charges, in general significantly different from Mulliken, are routinely used in force-field calculations of electrostatic interactions in protein environments and in aqueous solution.
[24] The propionate groups were taken as neutral in the calculation in order to allow comparison with synthetic heme analogs which also contain neutral groups. In heme proteins, these substituents are ionized at physiological pH and hydrogen bonded to nearby amino acid residues (C. L. Hunter, E. Lloyd, L. D. Eltis, S. P. Rafferty, H. Lee, M. Smith, A. G. Mauk, *Biochemistry* **1997**, *36*, 1010).
[25] W. A. Kalsbeck, A. Ghosh, R. K. Pandey, K. M. Smith, D. F. Bocian, *J. Am. Chem. Soc*. **1995**, *117*, 10959.
[26] F. Yang, G. N. Phillips, *J. Mol. Biol*. **1996**, *256*, 762.
[27] a) O. Lumpkin, W. T. Dixon, *J. Chem. Phys*. **1978**, *68*, 3485; b) O. K. Medhi, J. Silver, *Inorg. Chim. Acta* **1989**, *166*, 129.
[28] a) G. Lang, K. Spartalian, C. A. Reed, L. Collman, *J. Chem. Phys*. **1978**, *69*, 5424; b) H. Goff, G. N. La Mar, C. A. Reed, *J. Am. Chem. Soc*. **1977**, *77*, 3641; c) J. P. Collman, J. L. Hoard, N. Kim, G. Lang, C. A. Reed, *J. Am. Chem. Soc*. **1975**, *97*, 2676.
[29] a) N. Matsuzawa, M. Ata, D. A. Dixon, *J. Phys. Chem*. **1995**, *99*, 7698; b) B. Delley, *Physica B* **1991**, *172*, 185; P. M. Kozlowski, T. G. Spiro, M. Z. Zgierski, *J. Phys. Chem.* **1998**, *102*, 2603.
[30] T. A. Kent, K. Spartalian, G. Lang, *J. Chem. Phys* **1979**, *71*, 4899.
[31] a) M. Momenteau, J. Mispelter, B. Loock, J.-L. Lhoste, *J. Chem. Soc. Perkin Trans. I* **1985**, 221; M. Momenteau, J. Mispelter, B. Loock, J.-L. Lhoste, *J. Chem. Soc. Perkin Trans. I* **1985**, 61; b) H. Goof, G. N. La Mar, *J. Am. Chem. Soc*. **1977**, *99*, 6599; c) J. P. Collman, *Acc. Chem. Res.* **1977**, *10*, 265.
[32] The most distinctive features of the NMR and Mössbauer spectra are a large quadrupole splitting ($\Delta E_Q = 2-3$) in the former and a large contact shift of the pyrrolic protons (~30 ppm) in the latter.[4] Magnetic susceptibility measurements report a high magnetic moment (4.5–5.5 μ_B). To the best of our knowledge, EPR measurements on five-coordinate Fe^{II} systems are not available. Measurements done in mb and hb also give a high-spin iron (Fe out-of-planarity ~0.55 Å and $\mu \sim 5-5.5\ \mu_B$).

[33] a) S.-M. Peng, J. A. Ibers, *J. Am. Chem. Soc.* **1976**, *98*, 8032; b) C. Tetreau, D. Lavalette, M. Momenteau, J. Fischer, R. Weiss, *J. Am. Chem. Soc.* **1994**, *116*, 11840; c) D. Dolphin, J. R. Sams, T. B. Tsin, K. L. Wong, *J. Am. Chem. Soc.* **1976**, *98*, 6970.
[34] M. Paoli, G. Dodson , R. C. Liddington, A. J. Wilkinson, *J. Mol. Biol.* **1997**, *271*, 161.
[35] a) D. Harris, G. H. Loew, A. Komornicki, *J. Phys. Chem. A* **1997**, *101*, 3959; b) D. Harris, G. H. Loew, *J. Am. Chem. Soc.* **1996**, *108*, 10588.
[36] a) S. Obara, H. Kashiwagi, *J. Chem. Phys.* **1982**, *77*, 3155; b) D. C. Rawlings, M. Gouterman, E. R. Davidson, D. Feller, *Int. J. Quant. Chem.* **1985**, *28*, 823; c) H. Nakatsuji, J. Hasegawa, H. Ueda, M. Hada, *Chem. Phys. Lett.* **1996**, *250*, 379.
[37] a) F. Parak, E. W. Knapp, D. Kucheida, *J. Mol. Biol.* **1982**, *161*, 177; b) E. W. Knapp, S. E. Fisher, F. Parak, *J. Phys. Chem.* **1982**, *86*, 5042; c) X. Y. Li, M. Z. Zgierski, *Chem. Phys. Lett.* **1992**, *188*, 16.
[38] Note that, if one neglects the presence of the 2-me group in the axial imidazole, there are only two independent orientations for the O_2 ligand: the O–O axis projection in the same quadrant as the 2-meIm ligand ($1 = 1'$) or in a different quadrant ($2 = 2'$).
[39] a) O. Q. Munro, H. M. Marques, *Inorg. Chem.* **1996**, *35*, 3768; b) M. Maltempo, *J. Chem. Phys.* **1974**, *61*, 2540; c) S. Mitra, V. R. Marathe, R. Birdy, *Chem. Phys. Lett.* **1983**, *96*, 103; d) R. Birdy, D. V. Behere, S. Mitra, *J. Chem. Phys.* **1983**, *78*, 1453; e) K. Spartalian, G. Lang, C. A. Reed, *J. Chem. Phys.* **1979**, *71*, 1832.
[40] O. Kahn, *Molecular Magnetism*, VCH, New York, **1993**, p. 89.
[41] a) The preferred orientation of the 2-meIm ligand is a compromise between a maximum N_π–Fe_d bonding, achieved with an eclipsed conformation ($\Phi = 0^\circ$) and a minimum steric interaction with the Fe–N_p bonds, which is achieved in a bisecting conformation ($\Phi = 45^\circ$); b) W. R.Scheidt, D. M. Chipman, *J. Am. Chem. Soc.* **1986**, *108*, 1163.
[42] R. Hoffmann, M.-L. Chen, D. Thorn, *Inorg. Chem.* **1977**, *16*, 503.
[43] For a discussion of the electronic rearrangement when binding O_2 to [FeP] see refs. [19] and [42]. The same basic considerations hold here, with only slight differences in the d-Fe character of the orbitals due to the imidazole axial ligand. The notation $d\pi_1$, $d\pi_2$ refer to the $d_{xz} + d_{yz}$, $d_{xz} - d_{yz}$ combinations, respectively. $\pi^*_{g,s}$, $\pi^*_{g,a}$ refer to the two antibonding oxygen orbitals symmetric and antisymmetric, respectively, relative to the $(x + y, z)$ plane.
[44] The electron distribution can be schematized, in a more general case, as $(d_{xy})^{\uparrow\downarrow}(\mu_1 d\pi_1 + \mu_2 \pi^*_{g,s})^{\uparrow\downarrow}(\delta_1 \pi^*_{g,s} + \delta_2 d_{z^2} + \delta_3 n_{O_2})^{\uparrow\downarrow}(\lambda_1 d\pi_2 + \lambda_2 \pi^*_{g,a})^{\uparrow}$ $(\lambda_2 d\pi_2 + \lambda_1 \pi^*_{g,a})^{\downarrow}$. In the case of the bent structure, our computations give $\mu_1 \sim 1$, $\mu_2 \sim 0$; $\delta_1 \sim 1$, $\delta_2 \sim 0$, $\delta_3 \sim 0$; $\lambda_1 \sim 1$, $\lambda_2 \sim 0$.
[45] Note that the orbitals d_{xz}, d_{yz}, $\pi^*_{g,1}$, and $\pi^*_{g,2}$ of the linear conformation may turn into $d\pi_1$, $d\pi_2$, $\pi^*_{g,s}$, and $\pi^*_{g,a}$ in the bent conformation.
[46] C. Rovira, M. Parrinello, unpublished results.
[47] Neglecting the entropic contribution, one order of magnitude in equilibrium constant corresponds to approximately 1.5 kcal mol^{-1} difference in binding energy at 25 °C. Thus, a variation of 7 orders of magnitude in K_{eq} corresponds to $\sim$10 kcal mol^{-1} increase of binding energy.
[48] A simple approximation of the solvation energy can be derived from an Onsager model (L. Onsager, *J. Am. Chem. Soc.* **1936**, *58*, 1486). Equation (1) with the parameters $a = 10$ Å, $\varepsilon_o(EtOH) = 24$, μ_{calcd} $(PF) = 16$ D, μ_{calcd} $(PFO_2) = 10$ D, results in a solvation energy for the unligated system of double that of the six-coordinate system. This indicates a substantial reduction of the binding energy by solvation.

$$\Delta U = -\frac{2(\varepsilon_0 - 1)}{2\varepsilon_0 + 1}\frac{\mu^2}{a^3} \quad (1)$$

Received: February 26, 1998
Revised version: June 10, 1998 [F1029]

  0947-6539/99/0501-0262 $ 17.50+.50/0